P m r h s naHre f ha d er s Hs

Xin-Gang Zhao

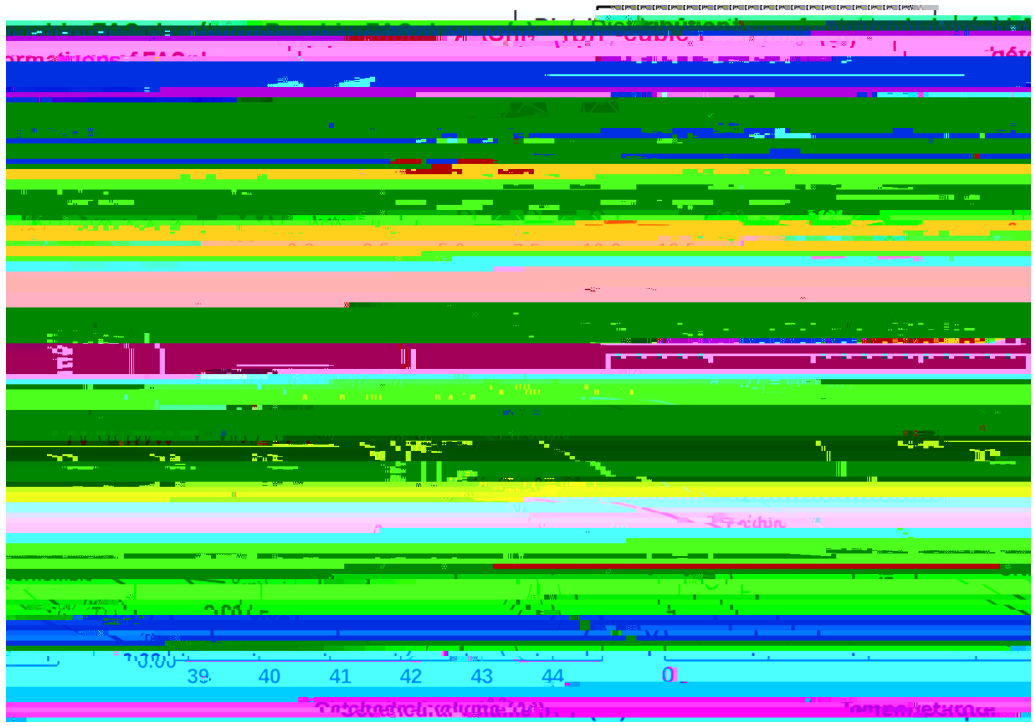

FIG. 1. Structures of monomorphous cubic (M-cubic) (a) and polymorphous cubic (P-cubic) (b) halide perovskite $FASnI_3$, and the distribution functions (c) of various octahedral deformations obtained by minimization of the internal energy in density functional supercell calculations. The panels in (c) show the distribution functions of octahedral titling along $x/y/z$ (top panel), B-site off-center displacement (middle panel), and the volumes of individual octahedra (bottom panel). Red and blue solid lines refer to polymorphous and monomorphous networks, respectively. The supercell structures were optimized by keeping fixed the cubic cell shape. (d) Schematics of the energies (enthalpy $\boldsymbol{H}$, Gibbs free energy $\boldsymbol{G}$) as function of temperature for cubic monomorphous phase (blue lines), cubic polymorphous (red lines) phase, and ground state orthorhombic (green lines) phase. The total energy lowering $\delta E^{(\text{P-M})}$ for the polymorphous cubic phase with respect to the cubic monomorphous phase was depicted with double arrow.

based on following gradients to the nearest local minimum) but is revealed once one initially applies a random atomic displacement ("nudge") off the cubic sites and explores lower symmetries in the minimization process.

The emerging physical picture is that the phase seen by XRD as cubic has in fact local structural motifs with low symmetries which emerge from the intrinsic low T chemical bonding pattern. This is different from ordinary inorganic compounds where reduced local symmetries emerge just from thermal disorder at elevated temperatures. The extensively discussed, single formula unit, cubic (Pm-3m) structure of halide perovskites [4,5,15,17–36] does not really exist, except as a macroscopically averaged fictitious structural model. Because x-ray diffraction has a rather long coherence length, such polymorphous systems were often fit in structure refinement models [16,37] by macroscopically averaged (fictitious monomorphous) cubic (Pm-3m) unit cells. Standard electronic structure calculations [4,15,17–28] that use input structures directly from crystal databases have often modeled the properties of the system (band gaps, absorption spectra, thermodynamic stability, alloy mixing enthalpies) as the property $\langle P \rangle = P(S_0)$ of the reported macroscopically averaged monomorphous structure [38,39] S_0 rather than the average $P_{\text{obs}} = \Sigma P(S_i)$ of the properties $\{P(S_i)\}$ of the individual, low symmetry microscopic configurations $\{S_i; i = 1, N\}$. One expects, as illustrated in this paper for a range of properties, that the properties $P(S_0)$ of the unphysical high symmetry cubic structure S_0

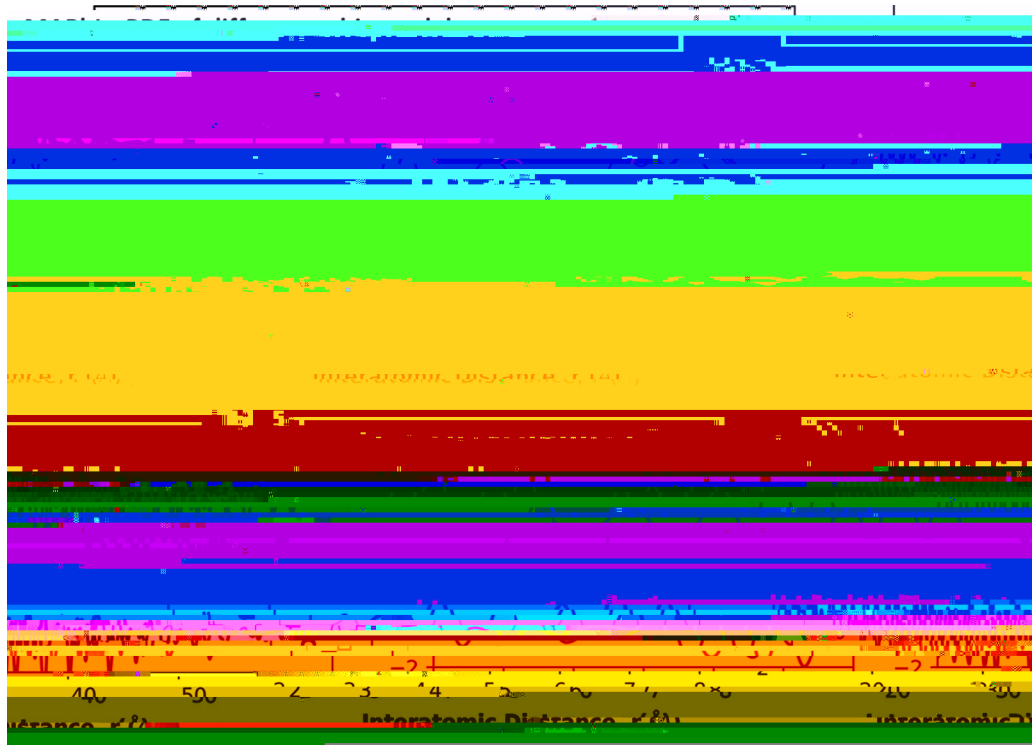

FIG. 2. Measured [40] [black line in (a)], and DFT-calculated [(a) and (b)] PDF, $G(r)$ for MAPbI

TABLE II. The differences ΔE_{tot} of total energy and ΔE_{g} (meV) of band gap between the large supercells with relaxation (polymorphous network) and the corresponding minimal cell structure (monomorphous approximation) by using PBE functional. The small positive values of ΔE_{tot} in the third and fourth columns are due to the numerical uncertainties (e.g., k mesh of different lattice types). The estimated uncertainty is 20–30 meV/

that the static relaxation and the physical properties calculated from different polymorphous realizations are robust.

IV. THE PDF OF THE ENERGY-MINIMIZING POLYMORPHOUS NETWORK

To examine if the energy minimizing geometry is realistic, we compare in Fig. 2 the *ab initio* calculated pair distribution function (PDF) with the experimental result [38] [shown by the black line in Fig. 2(a)], both for short and intermediate interatomic separations (left side panels) and long-range separations (right side panels).

Previous PDF measurements and simulations [60] often fit the data in a small unit cell by introducing parameters [40] such as atoms having nonspherical shapes, even changing the values of the observed lattice parameters, and altering Wyckoff positions with respect to XRD measurement in search for an effective model that fits the PDF. The ensuing structural models are generally nonperiodic, and the description of atoms as finite, shaped objects is incompatible with the way crystal structures are used as input in periodic band structure calculations. Thus, no bridge connects such

which is usually attributed to the thermal effect. Figure 4 also shows the comparison of the band gaps obtained from the polymorphous network ($T = 0$, minimization of the internal energy alone), with the band gaps obtained in the literature using finite temperature MD [6,42]. We used precisely the same exchange correlation functionals and lattice constants as in the respective MD calculations to assure consistency of the results. We see that the MD gaps are slightly higher but very similar to the P-cubic gaps, consistent with the view that the polymorphous structure derived from minimizing the *internal energy* captures the leading spectrum of distortions that control the band gaps at higher temperatures. Additional thermal disorder effects, introduced specifically by entropy, lead to an additional small increase in the band gap as temperature rises. In contrast to what Mladenović *et al.* [42] and Wiktor *et al.* [6] did (use a monomorphous structure at $T = 0$ as reference to calculate the renormalization energy with respect to the MD gap at high T), we define the renormalization energy as the difference of MD gap with respect to the polymorphous network. The latter approach we use gives ∼200 meV renormalization, very close to experiment, while the approach of Wiktor *et al.* [6] gives a 390–640 meV hig

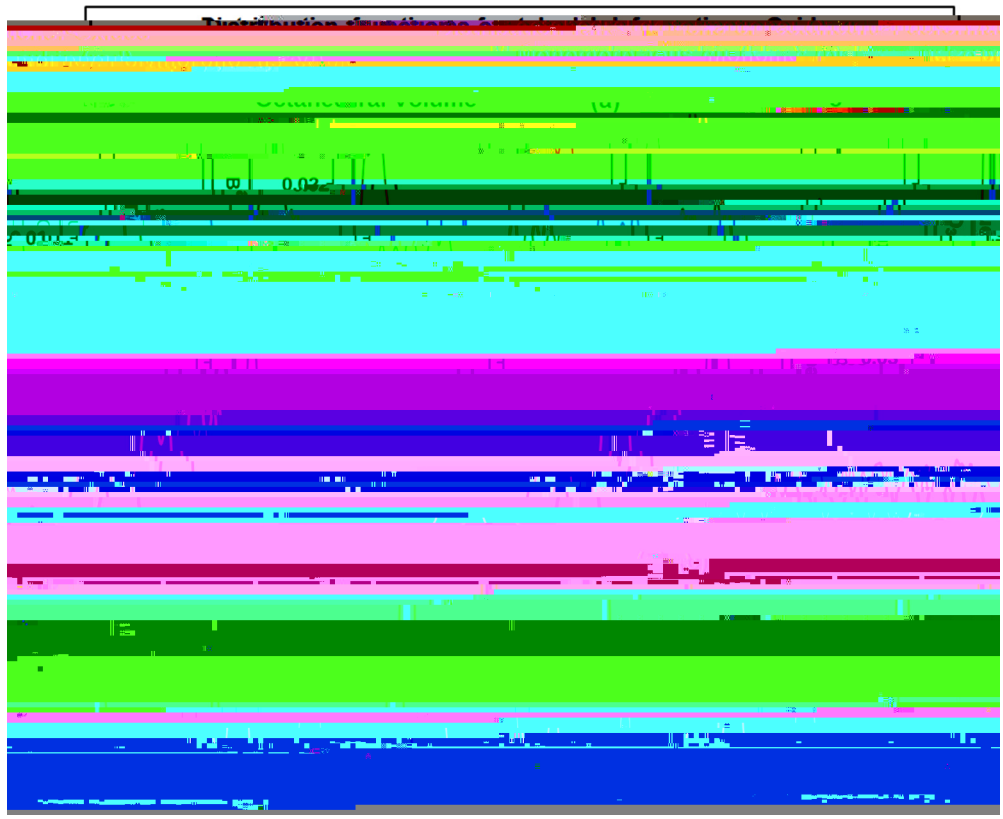

FIG. 7. Statistics of motifs in perovskites for (a) $BaTiO_3$ ($t = 0.94$), (b) $TlBiO_3$ ($t = 0.95$), and (c) $CsBiO_3$ ($t = 1.01$).

II. DISCUSSION OF THE CONTRIBUTION OF INTRINSIC ATHERMAL DISPLACEMENTS OF THERMAL DISORDER

This paper deals with a prototypical system with two phases, (a) the low temperature ground state (GS) structure (here orthorhombic or tetragonal for halide perovskites) that is a fully ordered structure at $T = 0$ K, and (b) the high temperature cubic phase. We are interested here primarily in the latter cubic phase, which is of general interest as a light-absorbing phase and shows a polymorphous network, whereas the low temperature ground state structure does not (see Table II showing no total energy lowering for the ground state as the cell increases). Each of the two phases is discussed in terms of by (i) its internal energy H that has but a small temperature dependence that will be neglected here, and (ii) its Gibbs free energy $G = H\text{-}TS$ that has an additional entropy-component $-TS$ of disorder when $T > 0$ K that is commonly described by molecular dynamics (MD) simulations [7–13].

The physics emerging from minimizing H. We first evaluate the properties of each of the two phases by constraining the unit cell shape to the phase of interest (tetragonal, cubic, others), and minimizing its respective H, described by DFT, as a function the cell-internal atomic positions. This provides the ideal low temperature atomic arrangements of the respective

energy H_{GS} by increasing its nominal cell size, i.e., this structure in inherently monomorphous.

The present paper studies the properties of the atomic position polymorphous network of a few cubic halide and oxide perovskites, including optical, dielectric, structural, and thermodynamic properties, finding that, relative to the virtual monomorphous structure, widely used in the literature a broad range of electronic structure calculations, use of the former removes many outstanding conflicts with experiment. This establishes such cubic phase of these compounds as being inherently *atomic-displacement polymorphous*, due to the nature of its chemical bonding. This draws an analogy with the recently discovered *spin configuration polymorphous networks*, characterizing paramagnetic ABO_3 "Mott insulators" with different local *spin* environments [75,76]. Indeed, the polymorphous network is not a model for approximate description but a physical structure. Yet a useful point is that the minimization of the internal energy under the constraint of macroscopically cubic phase provides a very useful approximate to the physical configuration. This can be used to calculate, with standard DFT codes, the structural properties (PDF, Fig. 2), band structure (Fig. 5), alloy physics (Fig. 6), band

FIG. 8. The calculated pair distribution function $G(r)$ as a function of interatomic distance (r

where $|Km\rangle$ is the mth electronic state at K in supercell Brillouin zone, and $|k_i n\rangle$ is the nth electronic state at k_i in the primitive Brillouin zone. One can then unfold the supercell band structure by calculating the spectral weight $P_{Km}(k_i$

FIG. 15. Band edges shift (VBM, CBM) due to octahedral tilting and B-site off-center in $CsPbI_3$ halide perovskite starting from monomorphous cubic (M-cubic) $CsPbI_3$ (middle). The potential energies were aligned by using core level of I-1*s* orbitals in monomorphous structure.

[Fig. 16(c)] cubic $FASnI_3$ indicates that the polymorphous cubic $FASnI_3$ presents sharply rising absorption.

We also compare the absorption coefficient of $MAPbI_3$ derived from $\alpha = 4\pi k/\lambda$ [Fig. 16(d), black line] using experimental extinction coefficient (k) [95] to our calculated results

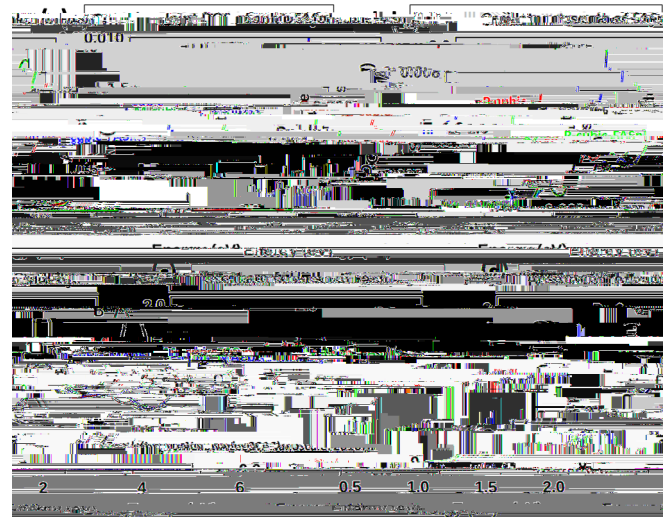

FIG. 16. The JDOS of the polymorphous and monomorphous (a) cubic $FASnI_3$. And the transition strength from valence bands to conduction bands for polymorphous (b) and monomorphous (c) cubic $FASnI_3$ structures. (d) Comparison of absorption between experimental absorption (solid black line) of pseudocubic $MAPbI_3$ [95] and calculated polymorphous cubic (solid red line, using Gaussian

[44] M. T. Weller, O. J. Weber, J. M. Frost, and A. Walsh, Cubic perovskite structure of black formamidinium lead iodide, α-$[HC(NH_2)_2]PbI_3$, at 298 K, J. Phys. Chem. Lett. **6**, 3209 (2015).

[45] R. J. Sutton, M. R. Filip, A. A. Haghighirad, N. Sakai, B. Wenger, F. Giustino, and H. J. Snaith, Cubic or orthorhombic? Revealing the crystal structure of metastable black-phase $CsPbI_3$ by theory of experiment, ACS Energy Lett. **3**, 1787 (2018).

[46] R. J. Worhatch, H. Kim, I. P. Swainson, A. L. Yonkeu, and S. J. L. Billinge, Study of local structure in selected organic–inorganic perovskites in the $Pm\bar{3}m$ phase, Chem. Mater. **20**, 1272 (2008).

[47] G. E. Eperon, S. D. Stranks, C. Menelaou, M. B. Johnston, L. M. Herz, and H. J. Snaith, Formamidinium lead trihalide: A broadly tunable perovskite for efficient planar heterojunction solar cells, Energy Environ. Sci. **7**, 982 (2014).

[48] C. C. Stoumpos, C. D. Malliakas, and M. G. Kanatzidis, Semiconducting tin of lead iodide perovskites with organic cations: Phase transitions, high mobilities, of near-infrared photoluminescent properties, Inorg. Chem. **52**, 9019 (2013).

[49] P. V. Balachandran, A. A. Emery, J. E. Gubernatis, T. Lookman,

iodide perovskite across the tetragonal–cubic structural phase transition, ChemSusChem **9**, 2692 (2016).

[74] J. Tilchin, D. N. Dirin, G. I. Maikov, A. Sashchiuk, M. V. Kovalenko, and E. Lifshitz, Hydrogen-like Wannier–Mott excitons in single crystal of methylammonium lead bromide perovskite, ACS Nano **10**, 6363 (2016).

[75] G. Trimarchi, Z. Wang, and A. Zunger, Polymorphous band structure model of gapping in the antiferromagnetic and paramagnetic phases of the Mott insulators MnO, FeO, CoO, and NiO, Phys. Rev. B **97**, 035107 (2018).

[76] J. Varignon, M. Bibes, and A. Zunger, Origin of band gaps in 3D perovskite oxides, Nat. Commun. **10**, 1658 (2019).

[77] H. Krakauer, R. Yu, C.-Z. Wang, K. M. Rabe, and U. V. Waghmare, Dynamic local distortions in $KNbO_3$, J. Phys.: Condens. Matter **11**, 3779 (1999).

[78] I. Ponomareva, L. Bellaiche, T. Ostapchuk, J. Hlinka, and J. Petzelt, Terahertz dielectric response of cubic $BaTiO_3$, Phys. Rev. B **77**, 012102 (2008).